



Removal of alachlor, diuron and isoproturon in water in a falling film dielectric barrier discharge (DBD) reactor combined with adsorption on activated carbon textile: Reaction mechanisms and oxidation by-products



Patrick Vanraes^{a,b,*}, Niels Wardenier^{b,c}, Pieter Surmont^d, Frederic Lynen^d, Anton Nikiforov^b, Stijn W.H. Van Hulle^c, Christophe Leys^b, Annemie Bogaerts^a

^a PLASMANT, Department of Chemistry, University of Antwerp, Campus Drie Eiken, Universiteitsplein 1, 2610 Wilrijk, Antwerp, Belgium

^b RUPT, Department of Applied Physics, Ghent University, Sint-Pietersnieuwstraat 41 B4, 9000 Ghent, Belgium

^c LIWET, Department of Industrial Biological Sciences, Ghent University, Campus Kortrijk, Graaf Karel de Goedelaan 5, 8500 Kortrijk, Belgium

^d Separation Science Group, Department of Organic and Macromolecular Chemistry, Ghent University, Krijgslaan 281 S4-bis, 9000 Gent, Belgium

ARTICLE INFO

Keywords:

Wastewater treatment
Advanced oxidation process
Aromatic micropollutants
Ozonation
Pesticides

ABSTRACT

A falling film dielectric barrier discharge (DBD) plasma reactor combined with adsorption on activated carbon textile material was optimized to minimize the formation of hazardous oxidation by-products from the treatment of persistent pesticides (alachlor, diuron and isoproturon) in water. The formation of by-products and the reaction mechanism was investigated by HPLC-TOF-MS. The maximum concentration of each by-product was at least two orders of magnitude below the initial pesticide concentration, during the first 10 min of treatment. After 30 min of treatment, the individual by-product concentrations had decreased to values of at least three orders of magnitude below the initial pesticide concentration. The proposed oxidation pathways revealed five main oxidation steps: dechlorination, dealkylation, hydroxylation, addition of a double-bonded oxygen and nitrication. The latter is one of the main oxidation mechanisms of diuron and isoproturon for air plasma treatment. To our knowledge, this is the first time that the formation of nitrified intermediates is reported for the plasma treatment of non-phenolic compounds.

1. Introduction

The increasing chemical pollution of both surface and ground water resources has become a global public concern as many related long-term effects on aquatic life and on human health are poorly understood [1]. Even at concentrations in the order of micrograms per liter and below, a wide spectrum of chemicals poses a potential risk due to their capacity to bio-accumulate and to persist in the environment, as well as their possible bioactivity [2]. In this context, agriculture is often considered to be a diffuse source of pesticides. Yet, pesticide transport towards surface water is complex and also occurs in urban areas [3], leading to a significant pesticide load on both rural and municipal wastewater treatment plants. Ongoing improvement of wastewater treatment has led to the development of methods termed advanced oxidation processes. They are defined as methods used to decompose target water pollutants by means of intermittent highly reactive species, such as ozone and hydroxyl radicals [4].

In the transfer of advanced oxidation processes towards real-world application, it is a major challenge to avoid hazardous oxidation by-products. The rise in transient toxicity during wastewater treatment has been observed in advanced oxidation processes for many types of micropollutants, in particular for the pesticides alachlor, diuron and isoproturon [5]. Moreover, the addition of activated carbon in advanced oxidation processes influences the formation of by-products by its catalytic effect on oxidants, its surface chemistry involving adsorbed compounds and its changing surface properties due to oxidation reactions [6,7]. In order to gain more insight into the associated risks, identification of intermediate degradation products is required and the main oxidation steps need to be revealed.

In our previous research, we have developed, characterized and optimized a new type of water treatment reactor, which combines oxidative treatment by dielectric barrier discharge (DBD) with micropollutant adsorption on activated carbon textile and with additional plasma gas bubbling [8,9]. The presence of an adsorptive material, such

* Corresponding author at: PLASMANT, Department of Chemistry, University of Antwerp, Campus Drie Eiken, Universiteitsplein 1, 2610 Wilrijk, Antwerp, Belgium.

E-mail addresses: patrick.vanraes@outlook.com (P. Vanraes), Niels.Wardenier@ugent.be (N. Wardenier), Pieter.Surmont@ugent.be (P. Surmont), Frederic.Lynen@ugent.be (F. Lynen), Anton.Nikiforov@ugent.be (A. Nikiforov), Stijn.VanHulle@ugent.be (S.W.H. Van Hulle), Christophe.Leys@ugent.be (C. Leys), Annemie.Bogaerts@uantwerpen.be (A. Bogaerts).

<https://doi.org/10.1016/j.jhazmat.2018.05.007>

Received 30 October 2017; Received in revised form 29 April 2018; Accepted 2 May 2018

Available online 03 May 2018

0304-3894/ © 2018 Elsevier B.V. All rights reserved.

as activated carbon, in a DBD reactor was shown to have a synergetic effect on micropollutant removal [10]. Moreover, a DBD reactor also allows for regeneration of the activated carbon [11] and thus prolongs the lifetime of the activated carbon. The present work focusses on the analysis of oxidation by-products from alachlor, diuron and isoproturon in the reactor by means of high-performance liquid chromatography time-of-flight mass spectrometry (HPLC-TOF-MS). The choice of these three pesticides is based on their toxicity [1,12,13], their worldwide occurrence as micropollutants in the environment [13–15], their persistence in the effluent of conventional wastewater treatment plants [16,17] and because of the ecological risk posed by their degradation by-products [13,14]. Oxidation experiments are performed with air plasma and the proposed oxidation pathways are subsequently compared with the cases of argon plasma and oxygen plasma, since these are commonly used working gases in studies on water treatment by plasma. More specifically, argon plasma is frequently chosen to gain more fundamental insight, due to its simple and well-characterized chemistry. The results are explained and discussed through insights from literature, together with the implications of this work on future research.

2. Experimental methods and materials

2.1. DBD water treatment reactor

Each pesticide decomposition experiment is performed with the plasma reactor described in our previous studies [8,9]. In short, a pesticide solution is continuously recirculated between a plasma chamber and an ozonation chamber. The plasma chamber consists of a coaxial DBD electrode system, where the grounded inner electrode is covered with one layer of Zorflex®, 100% activated carbon textile. The solution to be treated flows downwards along the carbon textile. Plasma is generated in dry air over the carbon textile by applying a pulsed AC high voltage on the outer mesh electrode that covers the tubular quartz glass dielectric barrier. In order to obtain uniform plasma treatment of the water film, the textile was carefully fixed to the inner electrode. In the ozonation chamber, the plasma generated ozone is bubbled through the solution for additional pesticide oxidation. Samples of the solution are taken from the ozonation chamber for micropollutant analysis at treatment times of 0, 2.5, 5, 10, 15, 20, 25 and 30 min. The reactor reference settings are given in Table 1. Information on the Zorflex® textile and on the method for power determination is provided in [8,9]. The initial solution of each micropollutant was made by dissolving 1.5 mg/L of the respective pesticide in deionized water. The experiments were repeated for initial concentrations of 30 mg/L, for additional confirmation of each detected oxidation by-product. Furthermore, the experiments were repeated with argon and oxygen as working gas, for comparison with dry air.

Table 1

Reactor reference settings for the experiments in this work.

Experimental parameter	Value
Voltage amplitude	7.9–8.4 kV
Input power	40 W
AC frequency	47.8 kHz
Modulation frequency	33.3 Hz
Duty cycle	15.0%
Treated volume	500 mL
Water flow rate	95.3 mL/min
Gas flow rate	1.00 SLM
Feed gas	air
Inter-electrode distance	2.25 mm
Initial micropollutant concentration	1.5 mg/L

2.2. Oxidation by-product analysis method

The oxidation by-products are determined by comparison of treated and untreated water samples by means of high-performance liquid chromatography coupled to diode array UV detection and time-of-flight mass spectrometry (HPLC-TOF-MS). For liquid-liquid extraction, a volume of 1.5 mL dichloromethane (CH_2Cl_2) was added to 45 mL water and the mixture was shaken for 5 min. Subsequently, 0.45 mL of the CH_2Cl_2 solution was extracted by means of a micropipette. Analysis was performed with an Agilent HPLC 1200 system consisting of a binary pump (Agilent Technologies, Waldbronn, Germany), a diode array detector (DAD) with a micro flow cell (volume: 1 mL, path length: 10 mm) and a 6230 time-of-flight mass spectrometer (TOF-MS) equipped with a Jetstream Electrospray Ionization source (ESI). Separations were conducted on a Luna C18 HPLC column (25 cm \times 2.1 mm \times 5 μm) equipped with a 2 mm C18 pre-column (SecurityGuard cartridge, Phenomenex). The mobile phase consisted of A: H_2O + 0.1% formic acid and B: Acetonitrile + 0.1% formic acid. A flow rate of 200 $\mu\text{L}/\text{min}$ was used. The initial conditions containing 2% B were held constant during 5 min, followed by a gradient up to 100% B in 50 min, a plateau of 100% during 10 min and back to initial in 2 min. Prior to each analysis series, the instrument was calibrated with the solution, following the procedure recommended by the manufacturer. In between analyses, the column was conditioned during 15 min. TOF-MS detection was performed in the positive jetstream electrospray ionization mode, using the following parameters: capillary 4000 V, nebulizer 30 psi, drying gas 8 L/min, gas temperature 300 °C, sheath gas 8 L/min, sheath gas temperature 300 °C, fragmentor 175 V, skimmer 66 V, OCT RF 750 V. Spectra were acquired from 50 to 1700 m/z at a scan rate of 1.02 s/spectrum. Lower masses were not measured, in order to limit noise in the measured data. All tests were carried out in duplicate with a regular blank solvent analysis, to ensure absence of cross contamination. The chromatograms are manually scanned for ions present in the treated samples and absent in the untreated sample. Identification of the ions is conducted with the molecular formula generator included in the Agilent Masshunter software. Since the molecular formula generator is not able to identify some of the detected ions, even for the high initial pesticide concentration of 30 mg/L, the likelihood of their identification is verified by the following additional data:

- the presence or absence of a Cl atom in the ion, which is deduced from the characteristic isotope abundance pattern;
- the experimental mass deviation Δppm ;
- the group-specific fragmentation pattern of the ions in electrospray ionization, which is determined by the abundance ratio and the difference in mass of the ions in a mass spectrum, in comparison to similar solutes (i.e. molecules with a similar molecular structure) measured at different retention times in the chromatogram. This relative abundance is calculated as the ratio of the corresponding peaks in the mass spectrum.

A mass deviation around $\Delta\text{ppm} \approx 15$ or higher is usually not tolerated by the molecular formula generator, although it is common when the abundance is either too high or too low. Group-specific fragmentation is found by comparison of the mass spectra of different solute molecules with each other and with literature data. Such an approach based on group-specific fragmentation in LC–MS for the best confidence in contaminant identification has been previously proposed by Niessen in his review on pesticide dissociation patterns [18].

3. Results and discussion

3.1. Alachlor oxidation by-products

Table 2 lists all detected ions that are associated to alachlor

Table 2

Proposed identification of alachlor and its by-products, eluting at a specified retention time (RT), as deduced from the corresponding detected parent and daughter ions measured in HPLC-TOF-MS detected in the sample of highest abundance (SHA). For each ion, identification is based, among others, on the Δ ppm value as calculated from the measured mass m_{exp} and theoretical mass m_{cal} , confirmation by the molecular formula generator (CMFG) and its relative abundance (RA) to the associated Na adduct ion.

SHA	RT (min)	name	formula	detected ion	m_{exp} (Da)	m_{cal} (Da)	Δ ppm	CMFG	RA (%)
0 min	44.3	1A	$\text{C}_{14}\text{H}_{20}\text{ClNO}_2$	$\text{C}_{14}\text{H}_{20}\text{ClNO}_2 \text{ Na}^+$	292.107	292.108	-3.5	yes	100
				$\text{C}_{13}\text{H}_{16}\text{ClNO} \text{ H}^+$	238.099	238.100	-3.6	yes	41
				$\text{C}_{11}\text{H}_{15}\text{N} \text{ H}^+$	162.127	162.128	-7.9	yes	32
				$\text{C}_{14}\text{H}_{20}\text{ClNO}_2 \text{ H}^+$	270.125	270.126	-4.0	yes	14
2.5 min	28.3	2A	$\text{C}_{12}\text{H}_{16}\text{ClNO}_3$	$\text{C}_{12}\text{H}_{16}\text{ClNO}_3 \text{ H}^+$	258.087	258.090	-11.6	yes	100
				$\text{C}_{14}\text{H}_{17}\text{NO}_5 \text{ Na}^+$	302.097	302.100	-11.4	yes	100
	33.8	2B	$\text{C}_{14}\text{H}_{17}\text{NO}_5$	$\text{C}_{14}\text{H}_{17}\text{NO}_5 \text{ H}^+$	280.115	280.118	-12.5	yes	49
				$\text{C}_{14}\text{H}_{20}\text{ClNO}_3 \text{ Na}^+$	308.107	308.103	13.2	yes	100
	36.6	2C	$\text{C}_{14}\text{H}_{20}\text{ClNO}_3$	$\text{C}_{13}\text{H}_{16}\text{ClNO}_2 \text{ H}^+$	254.097	254.095	8.7	no	28
				$\text{C}_{11}\text{H}_{15}\text{NO} \text{ H}^+$	178.125	178.123	10.2	no	16
				$\text{C}_{14}\text{H}_{20}\text{ClNO}_3 \text{ H}^+$	286.126	286.121	17.5	no	5
				$\text{C}_{14}\text{H}_{21}\text{NO}_3 \text{ Na}^+$	274.137	274.142	-17.9	yes	100
	37.5	2D	$\text{C}_{14}\text{H}_{21}\text{NO}_3$	$\text{C}_{14}\text{H}_{21}\text{NO}_3 \text{ H}^+$	252.153	252.160	-27.6	yes	21
				$\text{C}_{14}\text{H}_{20}\text{ClNO}_3 \text{ Na}^+$	308.106	308.103	9.9	yes	100
	38.1	2E	$\text{C}_{14}\text{H}_{20}\text{ClNO}_3$	$\text{C}_{13}\text{H}_{16}\text{ClNO}_2 \text{ H}^+$	254.098	254.095	12.7	yes	32
				$\text{C}_{11}\text{H}_{15}\text{NO} \text{ H}^+$	178.126	178.123	15.8	yes	11
$\text{C}_{14}\text{H}_{20}\text{ClNO}_3 \text{ H}^+$				286.125	286.121	14.0	yes	5	
$\text{C}_{14}\text{H}_{18}\text{ClNO}_4 \text{ Na}^+$				322.088	322.082	18.6	no	100	
5 min	32.9	3A	$\text{C}_{14}\text{H}_{18}\text{ClNO}_4$	$\text{C}_{13}\text{H}_{14}\text{ClNO}_3 \text{ H}^+$	268.077	268.074	11.0	no	19
				$\text{C}_{11}\text{H}_{13}\text{NO}_2 \text{ H}^+$	192.105	192.102	13.3	yes	17
				$\text{C}_{13}\text{H}_{18}\text{ClNO}_2 \text{ Na}^+$	278.096	278.092	14.4	yes	100
	34.6	3B	$\text{C}_{13}\text{H}_{18}\text{ClNO}_2$	$\text{C}_{12}\text{H}_{14}\text{ClNO} \text{ H}^+$	224.087	224.084	13.4	yes	103
				$\text{C}_{10}\text{H}_{13}\text{N} \text{ H}^+$	148.116	148.113	22.8	no	4
				$\text{C}_{14}\text{H}_{20}\text{ClNO}_4 \text{ Na}^+$	324.103	324.098	15.9	no	100
	35.5	3D	$\text{C}_{14}\text{H}_{20}\text{ClNO}_3$	$\text{C}_{13}\text{H}_{16}\text{ClNO}_3 \text{ H}^+$	270.093	270.090	12.2	no	33
				$\text{C}_{11}\text{H}_{15}\text{NO}_2 \text{ H}^+$	194.120	194.118	9.8	no	15
				$\text{C}_{14}\text{H}_{20}\text{ClNO}_3 \text{ Na}^+$	308.107	308.103	13.2	no	100
	35.8	3E	$\text{C}_{13}\text{H}_{16}\text{ClNO}_3$	$\text{C}_{13}\text{H}_{16}\text{ClNO}_2 \text{ H}^+$	254.098	254.095	12.7	no	22
				$\text{C}_{11}\text{H}_{15}\text{NO} \text{ H}^+$	178.124	178.123	4.6	no	5
				$\text{C}_{12}\text{H}_{14}\text{ClNO} \text{ H}^+$	224.087	224.084	12.4	no	44
	37.3	3G	$\text{C}_{14}\text{H}_{16}\text{ClNO}_4$	$\text{C}_{12}\text{H}_{16}\text{ClNO}_4 \text{ Na}^+$	296.070	296.066	13.5	no	100
				$\text{C}_{11}\text{H}_{12}\text{ClNO}_3 \text{ H}^+$	242.062	242.058	14.9	no	9
				$\text{C}_9\text{H}_{11}\text{NO}_2 \text{ H}^+$	166.091	166.087	25.3	yes	51
	37.3	3G	$\text{C}_{14}\text{H}_{16}\text{ClNO}_4$	$\text{C}_{14}\text{H}_{16}\text{ClNO}_4 \text{ Na}^+$	320.072	320.067	17.0	yes	100
				$\text{C}_{13}\text{H}_{14}\text{ClNO}_2 \text{ H}^+$	252.082	252.079	11.4	yes	39
				$\text{C}_{11}\text{H}_{13}\text{NO} \text{ H}^+$	176.110	176.108	14.0	yes	64
38.1	3H	$\text{C}_{14}\text{H}_{18}\text{ClNO}_3$	$\text{C}_{14}\text{H}_{18}\text{ClNO}_3 \text{ Na}^+$	306.093	306.087	18.7	yes	100	
			$\text{C}_{13}\text{H}_{14}\text{ClNO}_2 \text{ H}^+$	252.083	252.079	15.3	yes	14	
			$\text{C}_{11}\text{H}_{13}\text{NO} \text{ H}^+$	176.109	176.108	8.3	yes	33	
38.6	3I	$\text{C}_{14}\text{H}_{20}\text{ClNO}_6$	$\text{C}_{14}\text{H}_{20}\text{ClNO}_6 \text{ Na}^+$	356.092	356.088	12.1	yes	100	
			$\text{C}_{11}\text{H}_{15}\text{NO}_4 \text{ H}^+$	226.109	226.108	4.7	yes	7	
			$\text{C}_{14}\text{H}_{20}\text{ClNO}_6 \text{ H}^+$	334.109	334.106	9.8	no	6	
43.9	3J	$\text{C}_{14}\text{H}_{19}\text{ClN}_2\text{O}_5$	$\text{C}_{14}\text{H}_{19}\text{ClN}_2\text{O}_5 \text{ Na}^+$	353.088	353.088	0.0	yes	100	
			$\text{C}_{13}\text{H}_{15}\text{ClN}_2\text{O}_4 \text{ H}^+$	299.082	299.080	7.2	no	6	

oxidation by-products. It can thereby be noted that both proton (H^+) and sodium (Na^+) adducts are detected. The former, is related to the protic solvents and mobile phase additives used in the HPLC method. The latter, which could be considered an impurity, is inherent to the used HPLC-TOF-MS method in the positive ionization mode and originates mainly from the used glassware (such as the HPLC bottles) and from pollutant traces in the used Milli-Q® water. With the exception of molecules 2A, 2B and 2D, whose protonated and/or sodiated ions are not fragmented, and 3E and 3G, the fragmentation pattern observed for each proposed by-product is identical to the one suggested in [19] for electrospray ionization of alachlor. As an implication, the N-substituted branches in the parent ion are identical to the ones of alachlor, in agreement with the proposed molecular structures in Fig. 1. Note that not all possible isomer structures are represented for each by-product in Fig. 1. In particular, the exact position of hydroxyl groups on the aromatic ring or on the alkyl chains linked to the ring cannot be elucidated with the used techniques and remains therefore thus far unknown.

As the mass spectra of by-products 3E and 3G indicate, the methoxy function has been oxidized into formate, as displayed in Fig. 1. This is in

agreement with [20], where an identical oxidation mechanism is observed during ozonation of alachlor, as determined by means of collision-induced dissociation experiments. To our knowledge, Bouchonnet et al. were the first and only research group up to now to report this oxidation mechanism for alachlor.

With the exception of molecule 2A, all proposed by-product structural formulas are derived from alachlor by a combination of five types of oxidation steps:

- 1 Dechlorination by substitution of chloride with a hydroxyl group;
- 2 Hydroxylation by substitution of hydrogen with a hydroxyl group;
- 3 Oxidation by substitution of two hydrogen atoms with double bonded oxygen;
- 4 Dealkylation by substitution of an alkyl group with hydrogen;
- 5 Nitrification by substitution of hydrogen with a NO group (nitrosation) or NO_2 group (nitration).

The first four types are commonly encountered in ozonation and other advanced oxidation processes of organic compounds. Direct

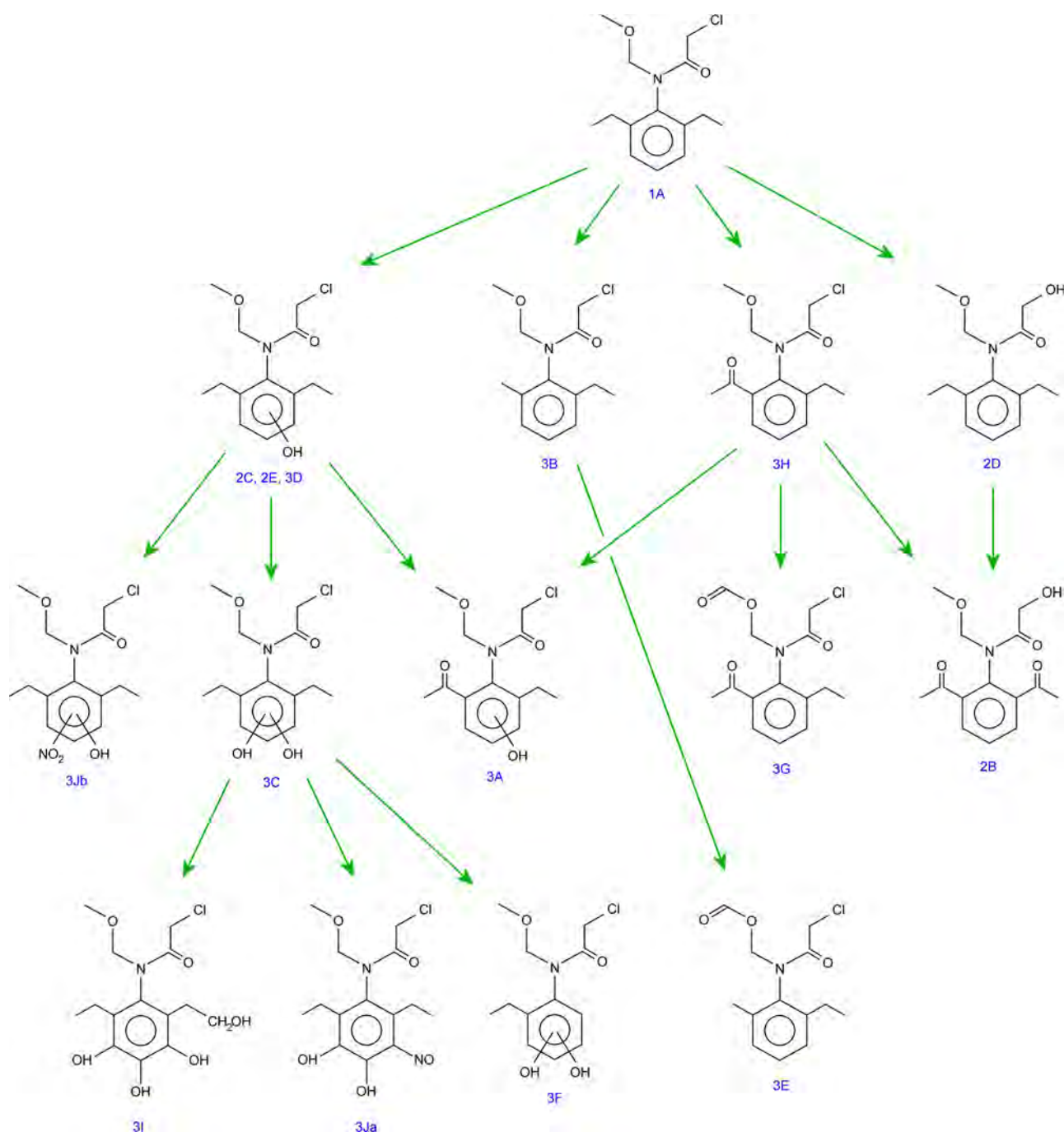


Fig. 1. Proposed oxidation pathway of alachlor under DBD plasma treatment in air.

oxidation by ozone is, however, a very selective process, in comparison to hydroxyl radical attack. Aromatic compounds with higher electron delocalization are known to exhibit higher reactivity towards ozonation [21,22]. This implies that O_3 attack is strongly electrophilic in nature and is preferably directed towards electron rich aromatic rings. Alterations of side-chains during ozonation, on the other hand, are mostly attributed to attack of OH radicals, which are produced from ozone hydrolysis [23].

Nitrication is uncommon in most advanced oxidation processes, as it requires the presence of reactive nitrogen species. Lukes et al. recently identified nitrified oxidation products of phenol after oxidation with plasma in air atmosphere [24]. They proposed several reaction pathways for both nitrosation and nitration. According to their model, nitrated by-products can be formed through attack of $NO_2\cdot$ or $NO\cdot$

radicals, nitrous and nitric acid in acidic conditions and decomposition of peroxyxynitrous acid in acid solution, while nitrosated by-products might result from $NO\cdot$ radical attack, reaction with a nitrosonium NO^+ ion under acidic conditions or direct attack by a peroxyxynitrite anion under alkaline conditions. To our knowledge, we are the first group to report experimental evidence on nitrication of non-phenolic micro-pollutants under plasma treatment in air. From our measurements on alachlor, however, it is unclear whether by-product 3J results from nitrosation (3Ja) or nitration (3Jb).

Fig. A.1 and Table A.1 in the Appendix show the removal progress of alachlor and its oxidation by-products. The estimated maximum concentration of each by-product is two to three orders of magnitude lower than the initial concentration of alachlor. After 30 min of treatment, only traces of 2A, 2C, 2E, 3B, 3D, 3H and 3J are detected, at

Table 3

Alachlor by-products observed in other advanced oxidation processes (AOPs) that have the same molecular formula as a few selected by-products in our measurements.

Isomers	Molecular formula	Oxidation step	AOP	References
3B	C ₁₃ H ₁₈ ClNO ₂	demethylation	ozonation electrochemical advanced oxidation Fenton-like oxidation	[27] [28] [29]
3E	C ₁₃ H ₁₆ ClNO ₃	demethylation + addition double bonded oxygen	ozonation hydrodynamic cavitation electrochemical advanced oxidation	[27] [26] [28]
2C, 2E, 3D	C ₁₄ H ₂₀ ClNO ₃	hydroxylation	ozonation peroxone ultrasonication photo-Fenton electrochemical advanced oxidation Fenton-like oxidation unassisted or H ₂ O ₂ -assisted heterogeneous photocatalysis	[25] [25] [30] [31] [28] [29] [32]
3H	C ₁₄ H ₁₈ ClNO ₃	addition double bonded oxygen	ozonation peroxone hydrodynamic cavitation permanganate-induced oxidation electrochemical advanced oxidation photocatalysis enhanced sono-Fenton process	[25,27] [25] [26] [25] [28] [33] [34]

estimated concentrations of at least three orders of magnitude below the original alachlor concentration. The five intermediates with highest abundance, 3H, 2E, 3D, 3B and 2C, are all found in the oxidation pathway of Fig. 1 as first generation oxidation by-products. The most abundant intermediate, 3H, is supposed to be formed by conversion of one of the ethyl side chains into an acetyl group. The exact same molecular structure was also identified through both GC–MS and HPLC–MS analysis as the main by-product in direct ozonation of alachlor as well as in the peroxone process [25]. Additionally, it has been reported as an oxidation product of alachlor in many other types of advanced oxidation processes (Table 3). This implies that 3H can be formed in our experiments through several oxidation mechanisms, such as direct attack by molecular ozone, and attack by a hydroxyl radical. Attack by an oxygen radical has also been proposed in literature as a possible reaction mechanism [26]. In only a few studies, an isomer of 3H is identified where the added double-bonded oxygen is positioned at a different location [20,25]. This suggests that oxidation of the ethyl side chain into an acetyl group is favored over many other oxidation steps.

Hydroxylation of alachlor into isomers such as 2C, 2E and 3D is another commonly reported oxidation step for many oxidation techniques (Table 3). Often, multiple isomers are detected in one study. For photocatalysis with TiO₂, the detected isomer is considered as one of the two main oxidation by-products [32]. In most research on alachlor oxidation, the exact location of the OH function is unknown and OH radical attack is proposed to occur to both the aromatic ring and the ethyl side chain. Next to that, also electrophilic attack of ozone on the benzene ring or on an ethyl group with formation of an OH function has been suggested [25].

An isomer of 3B and 3E, where the methyl group of the methoxy function is removed, has been reported as an alachlor by-product in all associated studies referred to in Table 3. Additionally, an isomer of 3G, in which the methoxymethyl group was kept intact, has been detected as a consequence of ozonation and peroxonation of alachlor in [25]. Therefore, addition of the two double-bonded oxygen atoms was suggested to be located on the ethyl side chains. All of these isomer structures, however, are in contradiction with the dissociation patterns of 3B, 3E and 3G measured in our experiments. The structural formulas of these three by-products as proposed in Fig. 1 are not found elsewhere in literature. Note in this regard that the methyl function in 3B and 3E possibly originates from an ethyl or –CH₂C(=O)H group, but that its formation from an acetyl group is improbable, considering the absence

of the latter oxidation step in other experimental oxidation studies, as well as in modeling studies, such as [35]. To our knowledge, also the chemical formulas of 2B, 3A, 3C, 3F, 3I and 3J in Table 2 have never been identified before as advanced oxidation by-products of alachlor.

For treatment with argon and oxygen plasma, all detected ions associated to alachlor oxidation by-products are given in Tables B.1 and B.2 in the Appendix. The corresponding proposed oxidation pathways are depicted in Fig. 2. As the pathways suggest, hydroxylation is favored under argon plasma, while it is less common under oxygen plasma. Furthermore, oxygen plasma promotes the addition of double bonded oxygen and also reveals higher dechlorination of alachlor. As expected, nitrification did not occur when using either an argon or oxygen plasma.

3.2. Diuron oxidation by-products

All detected ions that are associated to diuron oxidation by-products are listed in Table 4. Their removal progress and estimated concentration is presented in Table A.2 in the Appendix. The maximum abundance of each by-product is thereby two to three orders of magnitude smaller than the initial diuron abundance and their estimated final concentration after 30 min is at least four orders of magnitude below the initial diuron concentration. The mass spectrum of the main oxidation by-product 2B is in agreement with the one commonly reported in literature for N-demethyldiuron [36–40], which is the most frequently detected diuron by-product in advanced oxidation studies (Table 5). Interestingly, N-demethylation is considered to be the main oxidation step of several substituted phenylurea herbicides, including isoproturon, linuron, fluometuron and metoxuron, which all possess a similar N-substituted branch as diuron [37].

The proposed structural formulas of 2C, 3A and 3B correspond to first generation oxidation products formed by hydroxylation or nitration (Fig. 3). The isomers 3C and 4A are second generation oxidation by-products of diuron after one demethylation step and one nitration step (Fig. 3). As their mass spectrum suggests, substitution of an NO₂ group occurred during oxidation to the aromatic ring, most likely on an alpha carbon relative to the N-substituted branch.

As depicted in Fig. 3, the main oxidation steps in air plasma treatment of diuron according to our experiments are

- dechlorination,

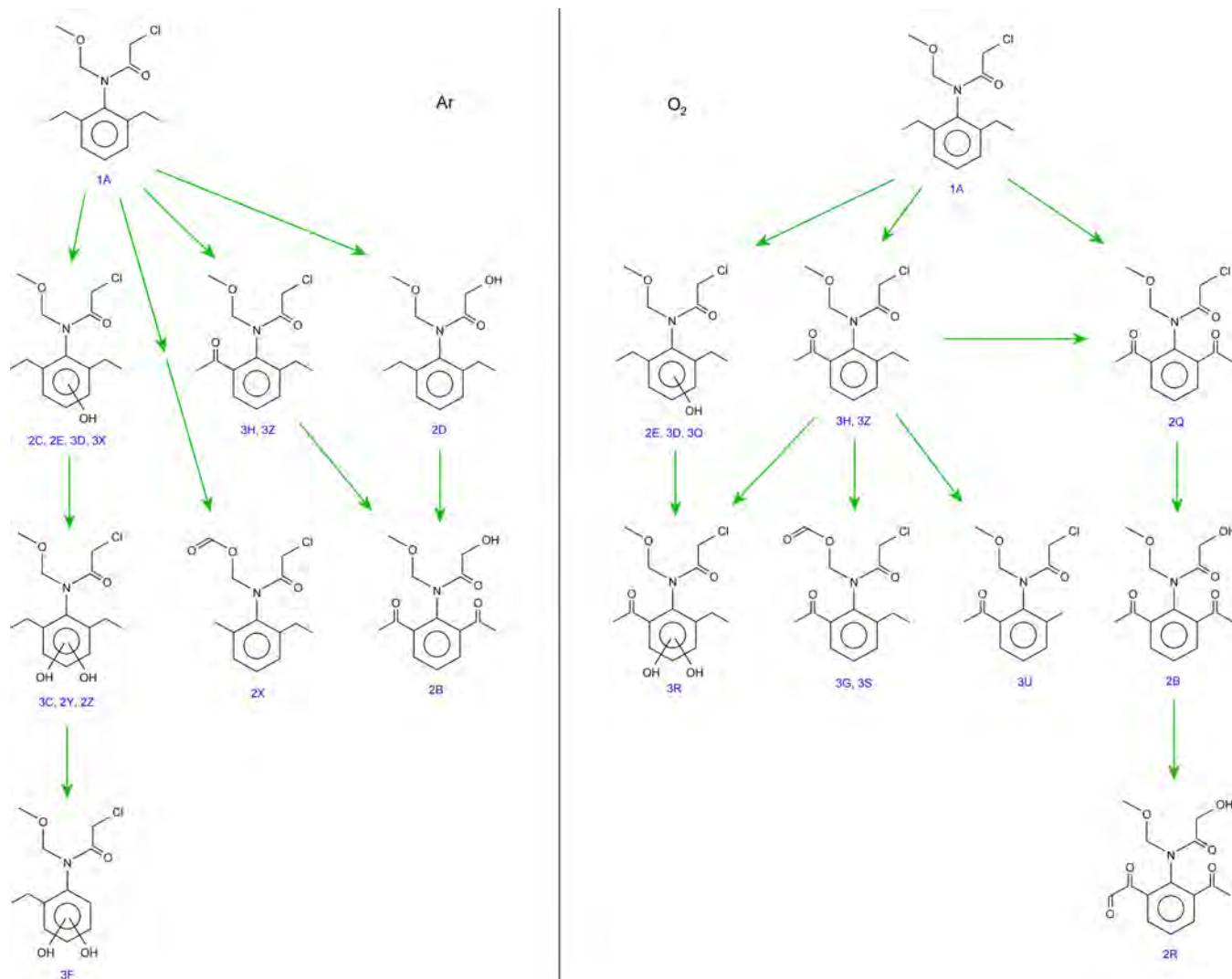


Fig. 2. Proposed oxidation pathway of alachlor under DBD plasma treatment in argon (left) and oxygen (right).

- hydroxylation,
- demethylation and
- nitrification.

Shankar et al. investigated by-product formation during photo-induced oxidation of diuron in aqueous solution by nitrites and nitrates [41]. Interestingly, they found two isomers with formula $C_9H_9Cl_2N_3O_3$ and two isomers with formula $C_8H_7Cl_2N_3O_3$ (Table 5). In all 4 cases, the fragmentation spectra in HPLC-analysis indicated nitrification of the aromatic ring, a process which was enhanced in NO_2^- conditions as opposed to NO_3^- conditions. The authors explained these observations with electrophilic attack of the ring by NO_2 radicals or the dimeric form N_2O_4 . NO_2 radical attack is also suggested in Lukes' model for nitration of phenol in air plasma treatment. If the dominant nitrification mechanism in our experiments is indeed electrophilic in nature, NO or NO_2 substitution will ideally occur on the aromatic cycle, at the ortho positions relative to the C–N bond, leading to the structural formulas of 2C, 3B, 3C and 4A as shown in Fig. 3. This is in agreement with the simulation results of Carrier et al., who calculated the location of preference for electrophilic attack on the diuron structure [42].

Similarly, hydroxylation by an electrophilic OH radical attack is expected to take place on the ring with a higher probability compared to a reaction on the methyl groups. Yet, such trend is not clearly observed experimentally. In advanced oxidation studies where

monohydroxylated diuron (3A) is measured, for instance, ring hydroxylation seems to be as likely as methyl hydroxylation, regardless of the type of AOP under consideration (Table 5). Either isomer has been reported as one of the three main diuron intermediates, e.g. in [38,44,49]. Carrier et al. performed TiO_2 -based photocatalysis on diuron and found four monohydroxylated diuron isomers [42]. Three isomers were attributed to OH substitution on the ring and one isomer to hydroxylation of a methyl function. Whereas OH attack of the aromatic cycle is a nucleophilic process, the methyl functions are assumed to be hydroxylated through hydrogen abstraction. Fig. 4a shows the stepwise transformation of one of the methyl groups into a hydroxymethyl or formyl function. First, attack of the methyl group by an OH radical leads to abstraction of one of the hydrogen atoms. Subsequent dioxygen attack results in a peroxy radical. Such radical is relatively stable and usually decays via bimolecular self-termination reactions to form a transient tetroxide which on its turn decomposes into an alcohol or aldehyde. To our knowledge, Mazzelier et al. were the first to postulate this mechanism for formyl formation in diuron [50].

Feng et al. conducted two studies on plasma treatment of diuron, with an AC powered DBD reactor [43] and with a pulsed bubble discharge reactor [54]. They reported several diuron intermediates in both studies with different alterations of the N-terminus. Accordingly, they proposed a stepwise mechanism for diuron demethylation, as presented in Fig. 4b. In this line of thought, by-product 3A can be a precursor of

Table 4

Proposed identification of diuron and its by-products, eluting at a specified retention time (RT), as deduced from the corresponding detected parent and daughter ions measured in HPLC-TOF-MS detected in the sample of highest abundance (SHA). For each ion, identification is based, among others, on the Δ ppm value as calculated from the measured mass m_{exp} and theoretical mass m_{cal} , confirmation by the molecular formula generator (CMFG) and its relative abundance (RA) to the associated ion of highest abundance.

SHA	RT (min)	name	formula	detected ion	m_{exp} (Da)	m_{cal} (Da)	Δ ppm	CMFG	RA (%)
0 min	36.9	1A	$\text{C}_9\text{H}_{10}\text{Cl}_2\text{N}_2\text{O}$	$\text{C}_9\text{H}_{10}\text{Cl}_2\text{N}_2\text{O H}^+$	233.024	233.025	-3.6	yes	100
				$\text{C}_9\text{H}_{10}\text{Cl}_2\text{N}_2\text{O Na}^+$	255.005	255.007	-7.0	yes	19
				$\text{C}_7\text{H}_3\text{Cl}_2\text{NO H}^+$	187.963	187.967	-21.2	yes	0.3
				$\text{C}_6\text{H}_3\text{Cl}_2\text{N H}^+$	159.968	159.972	-25.5	yes	0.2
2.5 min	26.9	2A	$\text{C}_9\text{H}_{11}\text{ClN}_2\text{O}_2$	$\text{C}_9\text{H}_{11}\text{ClN}_2\text{O}_2 \text{H}^+$	215.056	215.059	-12.7	yes	100
				$\text{C}_9\text{H}_{11}\text{ClN}_2\text{O}_2 \text{Na}^+$	237.038	237.041	-11.3	yes	44
	35.3	2B	$\text{C}_8\text{H}_8\text{Cl}_2\text{N}_2\text{O}$	$\text{C}_8\text{H}_8\text{Cl}_2\text{N}_2\text{O H}^+$	219.006	219.009	-14.6	yes	100
				$\text{C}_8\text{H}_8\text{Cl}_2\text{N}_2\text{O Na}^+$	240.988	240.991	-13.0	yes	11
				$\text{C}_6\text{H}_5\text{Cl}_2\text{N H}^+$	161.985	161.988	-16.9	yes	16
				$\text{C}_6\text{H}_5\text{ClN H}^+$	127.018	127.019	-6.9	yes	13
43.0	2C	$\text{C}_9\text{H}_9\text{Cl}_2\text{N}_3\text{O}_3$	$\text{C}_9\text{H}_9\text{Cl}_2\text{N}_3\text{O}_3 \text{H}^+$	278.011	278.010	3.9	yes	100	
			$\text{C}_9\text{H}_9\text{Cl}_2\text{N}_3\text{O}_3 \text{Na}^+$	299.993	299.992	3.8	yes	53	
5 min	36.6	3A	$\text{C}_9\text{H}_{10}\text{Cl}_2\text{N}_2\text{O}_2$	$\text{C}_9\text{H}_{10}\text{Cl}_2\text{N}_2\text{O}_2 \text{H}^+$	249.014	249.020	-23.1	yes	100
				$\text{C}_9\text{H}_{10}\text{Cl}_2\text{N}_2\text{O}_2 \text{Na}^+$	270.996	271.002	-21.0	yes	18
	36.9	3B	$\text{C}_9\text{H}_9\text{Cl}_2\text{N}_3\text{O}_3$	$\text{C}_9\text{H}_9\text{Cl}_2\text{N}_3\text{O}_3 \text{H}^+$	278.007	278.010	-10.5	yes	100
				$\text{C}_9\text{H}_9\text{Cl}_2\text{N}_3\text{O}_3 \text{Na}^+$	299.989	299.992	-9.5	yes	53
	40.1	3C	$\text{C}_8\text{H}_7\text{Cl}_2\text{N}_3\text{O}_3$	$\text{C}_8\text{H}_7\text{Cl}_2\text{N}_3\text{O}_3 \text{H}^+$	263.993	263.994	-4.8	no	6
				$\text{C}_6\text{H}_4\text{Cl}_2\text{N}_2\text{O}_2 \text{H}^+$	206.969	206.972	-14.5	yes	100
			$\text{C}_6\text{H}_2\text{Cl}_2\text{N}_2\text{O H}^+$	188.963	188.962	5.3	yes	31	
10 min	36.7	4A	$\text{C}_8\text{H}_7\text{Cl}_2\text{N}_3\text{O}_3$	$\text{C}_8\text{H}_7\text{Cl}_2\text{N}_3\text{O}_3 \text{H}^+$	263.995	263.994	2.8	yes	27
				$\text{C}_8\text{H}_7\text{Cl}_2\text{N}_3\text{O}_3 \text{Na}^+$	285.977	285.976	2.7	yes	27
				$\text{C}_6\text{H}_4\text{Cl}_2\text{N}_2\text{O}_2 \text{H}^+$	206.973	206.972	4.8	yes	100
				$\text{C}_6\text{H}_2\text{Cl}_2\text{N}_2\text{O H}^+$	188.963	188.962	5.3	yes	53

2B, on the condition that OH addition took place on one of the methyl groups. Next to such demethylation precursors, Feng et al. also detected one dechlorinated intermediate in their DBD reactor, in agreement with the identification of 2A in our measurements.

In our experiments, the abundance of each by-product decreases after 10 min of treatment and no new by-products are detected. As for

other advanced oxidation processes, opening of the aromatic ring is expected, with further decomposition into smaller organics, such as oxalic acid, oxamic acid, acetic acid and formic acid [38,55,56].

For argon and oxygen plasma, all detected ions associated to diuron oxidation by-products are given in Tables B.3 and B.4 in the Appendix. Under oxygen plasma, only by-product 2B is detected. The absence of

Table 5

Diuron by-products observed in other advanced oxidation processes (AOPs) that have the same molecular formula as a few selected by-products in our measurements.

Isomers	Molecular formula	Oxidation step	AOP	References
2B	$\text{C}_8\text{H}_8\text{Cl}_2\text{N}_2\text{O}$	demethylation	plasma treatment ozonation peroxonation photocatalytic ozonation UV/ H_2O_2 photolysis TiO_2 -based photocatalysis heterogeneous photocatalysis with N-doped titania photo-induced oxidation by nitrites and nitrates photocatalysis with ZnO photo-Fenton electro-Fenton ferrous-activated persulfate oxidation catalytic wet air oxidation	[43] [39,44–47] [46] [39] [45] [48] [37,38,42,49] [39] [41] [37] [38,50] [51] [40] [52]
2C, 3B	$\text{C}_9\text{H}_9\text{Cl}_2\text{N}_3\text{O}_3$	nitrification	photo-induced oxidation by nitrites and nitrates	[41]
3C, 4A	$\text{C}_8\text{H}_7\text{Cl}_2\text{N}_3\text{O}_3$	nitrification + demethylation	photo-induced oxidation by nitrites and nitrates	[41]
3A	$\text{C}_9\text{H}_{10}\text{Cl}_2\text{N}_2\text{O}_2$	ring hydroxylation	ozonation and UV/ H_2O_2 UV/ H_2O_2 TiO_2 -based photocatalysis photo-induced oxidation by nitrites and nitrates photo-Fenton electro-Fenton oxidation by chlorine dioxide plasma treatment ozonation photocatalytic ozonation TiO_2 -based photocatalysis photo-induced oxidation by nitrites and nitrates heterogeneous photocatalysis with N-doped titania photo-Fenton	[45] [45] [38,42] [41] [38] [51] [53] [43,54] [44] [39] [42,49] [41] [39] [55]
		methyl hydroxylation		

Table 6

Proposed identification of isotroturon and its by-products, eluting at a specified retention time (RT), as deduced from the corresponding detected parent and daughter ions measured in HPLC-TOF-MS detected in the sample of highest abundance (SHA). For each ion, identification is based, among others, on the Δ ppm value as calculated from the measured mass m_{exp} and theoretical mass m_{cal} , confirmation by the molecular formula generator (CMFG) and its relative abundance (RA) to the associated ion of highest abundance.

SHA	RT (min)	name	formula	detected ion	m_{exp} (Da)	m_{cal} (Da)	Δ ppm	CMFG	RA (%)
0 min	36.3	1A	$\text{C}_{12}\text{H}_{18}\text{N}_2\text{O}$	$\text{C}_{12}\text{H}_{18}\text{N}_2\text{O H}^+$	207.151	207.150	6.1	yes	100
				$\text{C}_{12}\text{H}_{18}\text{N}_2\text{O Na}^+$	229.133	229.132	5.8	yes	20
				$\text{C}_9\text{H}_{12}\text{N}_2\text{O H}^+$	165.103	165.103	1.3	yes	5
				$\text{C}_{10}\text{H}_{11}\text{NO H}^+$	162.091	162.091	0.0	yes	0.2
				$\text{C}_9\text{H}_{11}\text{N H}^+$	134.095	134.097	-14.7	yes	0.2
2.5 min	27.7	2A	$\text{C}_{12}\text{H}_{18}\text{N}_2\text{O}_3$	$\text{C}_{12}\text{H}_{18}\text{N}_2\text{O}_3 \text{H}^+$	239.143	239.140	14.4	no	100
				$\text{C}_{12}\text{H}_{18}\text{N}_2\text{O}_3 \text{Na}^+$	261.126	261.122	17.2	yes (low)	41
	32.5	2B	$\text{C}_{12}\text{H}_{18}\text{N}_2\text{O}_2$	$\text{C}_{12}\text{H}_{18}\text{N}_2\text{O}_2 \text{H}^+$	223.145	223.145	0.0	yes	100
				$\text{C}_{12}\text{H}_{18}\text{N}_2\text{O}_2 \text{Na}^+$	245.127	245.127	1.6	yes	29
	35.8	2C	$\text{C}_{12}\text{H}_{18}\text{N}_2\text{O}_2$	$\text{C}_{12}\text{H}_{18}\text{N}_2\text{O}_2 \text{H}^+$	223.145	223.145	0.0	yes	100
				$\text{C}_{12}\text{H}_{18}\text{N}_2\text{O}_2 \text{Na}^+$	245.127	245.127	1.6	yes	72
				$\text{C}_9\text{H}_{12}\text{N}_2\text{O}_2 \text{H}^+$	181.097	181.098	-3.9	yes	2
	38.1	2D	$\text{C}_{12}\text{H}_{17}\text{N}_3\text{O}_4$	$\text{C}_{12}\text{H}_{17}\text{N}_3\text{O}_4 \text{H}^+$	268.128	268.129	-3.7	yes	100
				$\text{C}_{12}\text{H}_{17}\text{N}_3\text{O}_4 \text{Na}^+$	290.111	290.111	0.0	yes	21
				$\text{C}_{10}\text{H}_{10}\text{N}_2\text{O}_4 \text{H}^+$	223.071	223.072	-4.0	yes	4
	38.7	2E	$\text{C}_{12}\text{H}_{17}\text{N}_3\text{O}_4$	$\text{C}_{12}\text{H}_{17}\text{N}_3\text{O}_4 \text{H}^+$	268.130	268.129	3.7	yes	100
				$\text{C}_{12}\text{H}_{17}\text{N}_3\text{O}_4 \text{Na}^+$	290.111	290.111	0.0	yes	30
				$\text{C}_9\text{H}_{12}\text{N}_2\text{O}_2 \text{H}^+$	181.097	181.098	-3.9	yes	13
	40.2	2F	$\text{C}_{12}\text{H}_{16}\text{N}_2\text{O}_2$	$\text{C}_{12}\text{H}_{15}\text{N}_3\text{O}_3 \text{H}^+$	250.119	250.119	-0.7	yes	20
				$\text{C}_{12}\text{H}_{16}\text{N}_2\text{O}_2 \text{H}^+$	221.128	221.129	-4.5	yes	100
				$\text{C}_{12}\text{H}_{16}\text{N}_2\text{O}_2 \text{Na}^+$	243.109	243.110	-4.1	yes	27
	42.4	2G	$\text{C}_{12}\text{H}_{17}\text{N}_3\text{O}_3$	$\text{C}_9\text{H}_{10}\text{N}_2\text{O}_2 \text{H}^+$	179.085	179.082	16.5	yes	3
				$\text{C}_{12}\text{H}_{17}\text{N}_3\text{O}_3 \text{H}^+$	252.134	252.134	0.0	yes	100
				$\text{C}_{12}\text{H}_{17}\text{N}_3\text{O}_3 \text{Na}^+$	274.115	274.116	-3.6	yes	57
	2H	$\text{C}_{12}\text{H}_{15}\text{N}_3\text{O}_4$	$\text{C}_{10}\text{H}_{10}\text{N}_2\text{O}_3 \text{H}^+$	207.077	207.077	0.2	yes	0.3	
$\text{C}_{12}\text{H}_{15}\text{N}_3\text{O}_4 \text{H}^+$			266.112	266.114	-7.5	yes	100		
$\text{C}_{12}\text{H}_{15}\text{N}_3\text{O}_4 \text{Na}^+$			288.095	288.096	-3.6	yes	55		
5 min	23.3	3A	$\text{C}_{12}\text{H}_{18}\text{N}_2\text{O}_2$	$\text{C}_{12}\text{H}_{18}\text{N}_2\text{O}_2 \text{H}^+$	223.148	223.145	13.4	yes	100
				$\text{C}_{12}\text{H}_{18}\text{N}_2\text{O}_2 \text{Na}^+$	245.131	245.127	18.0	yes	57
				$\text{C}_9\text{H}_{12}\text{N}_2\text{O Na}^+$	165.106	165.103	19.5	no	4
	26.2	3B	$\text{C}_{10}\text{H}_{14}\text{N}_2\text{O}_3$	$\text{C}_{10}\text{H}_{14}\text{N}_2\text{O}_3 \text{H}^+$	211.112	211.108	18.9	yes	100
				$\text{C}_{10}\text{H}_{14}\text{N}_2\text{O}_3 \text{Na}^+$	233.094	233.090	17.2	yes	53
	29.9	3C	$\text{C}_{11}\text{H}_{16}\text{N}_2\text{O}_3$	$\text{C}_{11}\text{H}_{16}\text{N}_2\text{O}_3 \text{H}^+$	225.126	225.124	9.3	yes	20
				$\text{C}_{11}\text{H}_{16}\text{N}_2\text{O}_3 \text{Na}^+$	247.108	247.105	12.1	yes	100
	31.2	3D	$\text{C}_{12}\text{H}_{17}\text{N}_3\text{O}_4$	$\text{C}_{12}\text{H}_{17}\text{N}_3\text{O}_4 \text{H}^+$	268.133	268.129	14.9	no	100
				$\text{C}_{12}\text{H}_{17}\text{N}_3\text{O}_4 \text{Na}^+$	290.115	290.111	13.8	no	89
	31.7	3E	$\text{C}_{12}\text{H}_{17}\text{N}_3\text{O}_4$	$\text{C}_{12}\text{H}_{17}\text{N}_3\text{O}_4 \text{H}^+$	268.133	268.129	14.9	yes	99
				$\text{C}_{12}\text{H}_{17}\text{N}_3\text{O}_4 \text{Na}^+$	290.115	290.111	13.8	yes	100
	34.6	3F	$\text{C}_{11}\text{H}_{16}\text{N}_2\text{O}$	$\text{C}_{11}\text{H}_{16}\text{N}_2\text{O H}^+$	193.136	193.134	9.9	yes	100
				$\text{C}_{11}\text{H}_{16}\text{N}_2\text{O Na}^+$	215.117	215.116	4.5	yes	58
				$\text{C}_8\text{H}_{10}\text{N}_2\text{O H}^+$	151.087	151.087	0.0	yes	10
	36.9	3G	$\text{C}_{12}\text{H}_{17}\text{N}_3\text{O}_4$	$\text{C}_9\text{H}_{13}\text{N H}^+$	136.112	136.113	-4.6	yes	3
				$\text{C}_{12}\text{H}_{17}\text{N}_3\text{O}_4 \text{H}^+$	268.129	268.129	0.0	yes	74
				$\text{C}_{12}\text{H}_{17}\text{N}_3\text{O}_4 \text{Na}^+$	290.111	290.111	0.0	yes	100
39.4	3H	$\text{C}_{11}\text{H}_{15}\text{N}_3\text{O}_3$	$\text{C}_{11}\text{H}_{15}\text{N}_3\text{O}_3 \text{H}^+$	238.117	238.119	-9.1	yes	10	
			$\text{C}_{11}\text{H}_{15}\text{N}_3\text{O}_3 \text{Na}^+$	260.100	260.101	-4.3	yes	16	
			$\text{C}_9\text{H}_{12}\text{N}_2\text{O}_2 \text{H}^+$	181.098	181.098	1.6	yes	100	
			$\text{C}_9\text{H}_{10}\text{N}_2\text{O H}^+$	163.087	163.087	0.0	yes	18	
			$\text{C}_6\text{H}_6\text{N}_2\text{O}_2 \text{H}^+$	139.049	139.051	-12.6	yes	1	
$\text{C}_6\text{H}_4\text{N}_2\text{O H}^+$	121.039	121.040	-9.8	yes	2				

comparison to by-products formed by any other oxidation step. As this indicates, nitrification is either the most frequent oxidation step or it produces the most recalcitrant intermediates. In other studies on advanced oxidation of isotroturon, on the other hand, hydroxylation clearly is the most frequent degradation mechanism. Singly hydroxylated isotroturon, such as 2B, 2C and 3A, for instance, is the most commonly encountered by-product (Table 7). Three separate studies identified three isomers, of which two underwent OH substitution on the ring and one at the isopropyl group [57–59]. Amorisco et al., Losito et al. and López-Muñoz et al. made more profound by-product studies for TiO_2 -based photocatalysis and found substitution of H with OH to occur at basically every possible location: on the ring, in the isopropyl and dimethyl amide groups and even at the secondary amide function [60–62].

In contrast to diuron, transformation of a methyl into a formyl

group is observed in our experiments for isotroturon by-product 2F, in the dimethyl amide function. This by-product has only been reported before in two studies (Table 7). Also here, formation of a hydroxymethyl or formyl function is postulated to proceed with H abstraction as depicted in Fig. 4a. Besides, multiple authors support the demethylation mechanism of Fig. 4b for isotroturon [59,60]. Single demethylation in the dimethyl amide function, resulting in 3F, has been observed in four other studies (Table 7). Remarkably, dealkylation in the isopropyl function is mostly accompanied by replacement with OH, while this is rather an exception in the dimethyl amide function.

4. Conclusion

We analyzed the oxidation by-products ofalachlor, diuron and isotroturon in a falling water film DBD reactor with activated carbon

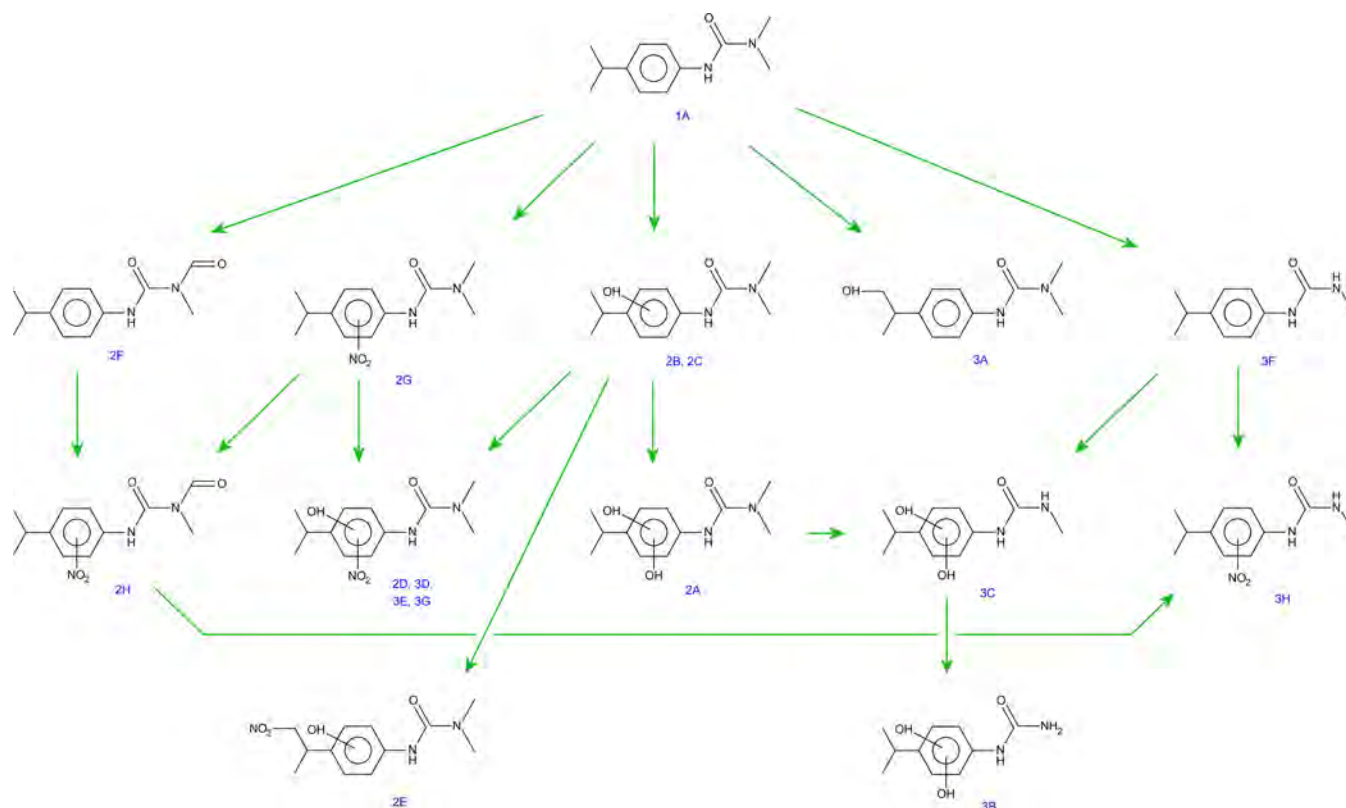


Fig. 5. Proposed oxidation pathway of isoproturon under the DBD plasma treatment in an air atmosphere as used in this work.

Table 7

Isoproturon by-products observed in other advanced oxidation processes (AOPs) that depict the same molecular formula as a few selected by-products in our measurements.

Isomers	Molecular formula	Oxidation step	AOP	References
2B, 2C, 3A	$C_{12}H_{18}N_2O_2$	hydroxylation	ozonation oxidation with NaClO oxidation with ClO_2 electro-Fenton TiO_2 -based photocatalysis	[57] [58,63] [53,63] [61] [59–62]
2F	$C_{12}H_{16}N_2O_2$	addition double bonded oxygen	peroxonation TiO_2 -based photocatalysis	[64] [62]
3F	$C_{11}H_{16}N_2O$	demethylation	TiO_2 -based photocatalysis electro-Fenton	[59,60,62] [61]

textile, by means of HPLC-TOF-MS. The oxidation pathways for the three plasma gases, i.e. air, argon and oxygen, are presented. In the case of air plasma, intermediates are predominantly formed through five types of oxidation steps: dechlorination, hydroxylation, addition of double bonded oxygen, dealkylation and nitrification. For argon and oxygen plasmas, nitrification does not occur, as expected. Although the exact site of oxidation is unknown for the majority of by-products, the mass spectra often provide clear indications of which part in the molecular structure is affected. While the aromatic ring is theoretically expected to be the oxidation site of preference, oxidation of the side chains is detected as well, in good agreement with other studies on advanced oxidation. This is the first study, to our knowledge, where nitrification of non-phenolic micropollutants through NO and NO_2 radical attack by means of plasma treatment is detected. Remarkably, it is

one of the major oxidation steps for diuron and isoproturon, while only one minor nitrified by-product of alachlor is tentatively identified. As should be noted, nitrification is mainly observed on hydroxylated by-products. Toxicity analysis of nitrified intermediates is an important topic for future research to understand the feasibility of air plasma for water purification. A solution to prevent the generation of toxic nitrified by-products in industrial applications could be found in the use of an oxygen based plasma instead of an air plasma.

Acknowledgments

This research did not receive any specific grant from funding agencies in the public, commercial, or not-for-profit sectors. The authors would like to thank Carbon Cloth Division for Zorflex® samples and personally thank Jack Taylor for fruitful discussion of active carbon water treatment processes.

Appendix A. Supplementary data

Supplementary material related to this article can be found, in the online version, at doi:<https://doi.org/10.1016/j.jhazmat.2018.05.007>.

References

- [1] S. Hussain, M. Devers-Lamrani, N. El Azhari, F. Martin-Laurent, Isolation and characterization of an isoproturon mineralizing *Sphingomonas* sp. strain SH from a French agricultural soil, *Biodegradation* 22 (2011) 637–650.
- [2] C.G. Campbell, S.E. Borglin, F.B. Green, A. Grayson, E. Wozel, W.T. Stringfellow, Biologically directed environmental monitoring, fate, and transport of estrogenic endocrine disrupting compounds in water: a review, *Chemosphere* 65 (2006) 1265–1280.
- [3] A.C. Gerecke, M. Schärer, H.P. Singer, S.R. Müller, R.P. Schwarzenbach, M. Sägger, U. Ochsenbein, G. Popow, Sources of pesticides in surface waters in Switzerland: pesticide load through waste water treatment plants—current situation and reduction potential, *Chemosphere* 48 (2002) 307–315.
- [4] C. Comninellis, A. Kapalka, S. Malato, S.A. Parsons, I. Poullos, D. Mantzavinos, Advanced oxidation processes for water treatment: advances and trends for R&D, *J. Chem. Technol. Biotechnol.* 83 (2008) 769–776.

- [5] M.B. Kralj, P. Trebše, M. Franko, Applications of bioanalytical techniques in evaluating advanced oxidation processes in pesticide degradation, *TrAC Trends Anal. Chem.* 26 (2007) 1020–1031.
- [6] P. Alvarez, J. García-Araya, F. Beltrán, I. Giráldez, J. Jaramillo, V. Gómez-Serrano, The influence of various factors on aqueous ozone decomposition by granular activated carbons and the development of a mechanistic approach, *Carbon* 44 (2006) 3102–3112.
- [7] E. Paternina, J.M. Arias, D. Barragán, Kinetic study of the catalyzed decomposition of hydrogen peroxide on activated carbon, *Quím. Nova* 32 (2009) 934–938.
- [8] P. Vanraes, H. Ghodbane, D. Davister, N. Wardenier, A. Nikiforov, Y.P. Verheust, S.W. Van Hulle, O. Hamdaoui, J. Vandamme, J. Van Durme, Removal of several pesticides in a falling water film DBD reactor with activated carbon textile: energy efficiency, *Water Res.* 116 (2017) 1–12.
- [9] P. Vanraes, G. Willems, A. Nikiforov, P. Surmont, F. Lynen, J. Vandamme, J. Van Durme, Y.P. Verheust, S.W.H. Van Hulle, A. Dumoulin, C. Leys, Removal of atrazine in water by combination of activated carbon and dielectric barrier discharge, *J. Hazard. Mater.* 299 (2015) 647–655.
- [10] P. Vanraes, G. Willems, N. Daels, S.W. Van Hulle, K. De Clerck, P. Surmont, F. Lynen, J. Vandamme, J. Van Durme, A. Nikiforov, Decomposition of atrazine traces in water by combination of non-thermal electrical discharge and adsorption on nanofiber membrane, *Water Res.* 72 (2015) 361–371.
- [11] S. Tang, N. Lu, J. Li, Y. Wu, Design and application of an up-scaled dielectric barrier discharge plasma reactor for regeneration of phenol-saturated granular activated carbon, *Sep. Purif. Technol.* 95 (2012) 73–79.
- [12] S. Weichenthal, C. Moase, P. Chan, A review of pesticide exposure and cancer incidence in the agricultural health study cohort, *Environ. Health Perspect.* 118 (2010) 1117–1125.
- [13] S. Giacomazzi, N. Cochet, Environmental impact of diuron transformation: a review, *Chemosphere* 56 (2004) 1021–1032.
- [14] E. Thurman, D. Goolsby, D. Aga, M. Pomes, M. Meyer, Occurrence of alachlor and its sulfonated metabolite in rivers and reservoirs of the Midwestern United States: the importance of sulfonation in the transport of chloroacetanilide herbicides, *Environ. Sci. Technol.* 30 (1996) 569–574.
- [15] I.S. Fomsgaard, N.H.H. Spliid, G. Felding, Leaching of pesticides through normal-tillage and low-tillage soil—a lysimeter study. I. Isoproturon, *J. Environ. Sci. Health: Part B* 38 (2003) 1–18.
- [16] N. Barco-Bonilla, R. Romero-González, P. Plaza-Bolaños, J.L. Martínez Vidal, A. Garrido Frenich, Systematic study of the contamination of wastewater treatment plant effluents by organic priority compounds in Almería province (SE Spain), *Sci. Total Environ.* 447 (2013) 381–389.
- [17] R. Loos, R. Carvalho, D.C. António, S. Comerio, G. Locoro, S. Tavazzi, B. Paracchini, M. Ghiani, T. Lettieri, L. Blaha, B. Jarosova, S. Voorspoels, K. Servaes, P. Haglund, J. Fick, R.H. Lindberg, D. Schwesig, B.M. Gawlik, EU-wide monitoring survey on emerging polar organic contaminants in wastewater treatment plant effluents, *Water Res.* 47 (2013) 6475–6487.
- [18] W.M.A. Niessen, Group-specific fragmentation of pesticides and related compounds in liquid chromatography–tandem mass spectrometry, *J. Chromatogr. A* 1217 (2010) 4061–4070.
- [19] D. Volmer, A. Preiss, K. Levsen, G. Wünsch, Thermospray mass spectral studies of pesticides: temperature and salt concentration effects on the ion abundances in thermospray mass spectra, *J. Chromatogr. A* 647 (1993) 235–259.
- [20] S. Bouchonnet, S. Kinani, Y. Souissi, S. Bourcier, M. Sablier, P. Roche, V. Boireau, V. Ingrand, Investigation of the dissociation pathways of metolachlor, acetochlor and alachlor under electron ionization—application to the identification of ozonation products, *Rapid Commun. Mass Spectrom.* 25 (2011) 93–103.
- [21] C. Decoret, J. Royer, B. Legube, M. Dore, Experimental and theoretical studies of the mechanism of the initial attack of ozone on some aromatics in aqueous medium, *Environ. Technol.* 5 (1984) 207–218.
- [22] J. Hoigné, H. Bader, Rate constants of reactions of ozone with organic and inorganic compounds in water—I: non-dissociating organic compounds, *Water Res.* 17 (1983) 173–183.
- [23] K.S. Tay, N.A. Rahman, M.R.B. Abas, Ozonation of parabens in aqueous solution: kinetics and mechanism of degradation, *Chemosphere* 81 (2010) 1446–1453.
- [24] P. Lukes, E. Dolezalova, I. Sisrova, M. Clupek, Aqueous-phase chemistry and bactericidal effects from an air discharge plasma in contact with water: evidence for the formation of peroxyxynitrite through a pseudo-second-order post-discharge reaction of H₂O₂ and HNO₂, *Plasma Sources Sci. Technol.* 23 (2014) 015019.
- [25] Z. Qiang, C. Liu, B. Dong, Y. Zhang, Degradation mechanism of alachlor during direct ozonation and O₃/H₂O₂ advanced oxidation process, *Chemosphere* 78 (2010) 517–526.
- [26] X. Wang, Y. Zhang, Degradation of alachlor in aqueous solution by using hydrodynamic cavitation, *J. Hazard. Mater.* 161 (2009) 202–207.
- [27] H.-y. Li, J.-h. Qu, H.-j. Liu, Decomposition of alachlor by ozonation and its mechanism, *J. Environ. Sci.* 19 (2007) 769–775.
- [28] A.R. Pipi, A.R. De Andrade, E. Brillas, I. Sires, Total removal of alachlor from water by electrochemical processes, *Sep. Purif. Technol.* 132 (2014) 674–683.
- [29] J. Bolobajev, M. Trapido, A. Goi, Improvement in iron activation ability of alachlor Fenton-like oxidation by ascorbic acid, *Chem. Eng. J.* 281 (2015) 566–574.
- [30] D.G. Wayment, D.J. Casadonte, Frequency effect on the sonochemical remediation of alachlor, *Ultrason. Sonochem.* 9 (2002) 251–257.
- [31] H. Katsumata, S. Kaneco, T. Suzuki, K. Ohta, Y. Yobiko, Photo-Fenton degradation of alachlor in the presence of citrate solution, *J. Photochem. Photobiol. A: Chem.* 180 (2006) 38–45.
- [32] W. Chu, C. Wong, Study of herbicide alachlor removal in a photocatalytic process through the examination of the reaction mechanism, *Ind. Eng. Chem. Res.* 43 (2004) 5027–5031.
- [33] Y.-K. Chang, Y.-S. Wu, C.-S. Lu, P.-F. Lin, T.-Y. Wu, Photodegradation of alachlor using BiVO₄ photocatalyst under visible light irradiation, *Water Air Soil Pollut.* 226 (2015).
- [34] C. Wang, Z. Liu, Degradation of alachlor using an enhanced sono-Fenton process with efficient Fenton's reagent dosages, *J. Environ. Sci. Health: Part B* 50 (2015) 504–513.
- [35] Y. Gao, Y. Ji, G. Li, B. Mai, T. An, Bioaccumulation and ecotoxicity increase during indirect photochemical transformation of polycyclic musk tonalide: a modeling study, *Water Res.* 105 (2016) 47–55.
- [36] K. Abass, P. Reponen, M. Turpeinen, J. Jalonen, O. Pelkonen, Characterization of diuron N-demethylation by mammalian hepatic microsomes and cDNA-expressed human cytochrome P450 enzymes, *Drug Metab.* 35 (2007) 1634–1641.
- [37] J. Fenoll, P. Sabater, G. Navarro, G. Pérez-Lucas, S. Navarro, Photocatalytic transformation of sixteen substituted phenylurea herbicides in aqueous semiconductor suspensions: intermediates and degradation pathways, *J. Hazard. Mater.* 244–245 (2013) 370–379.
- [38] S. Malato, J. Cáceres, A. Fernández-Alba, L. Piedra, M. Hernando, A. Agüera, J. Vial, Photocatalytic treatment of diuron by solar photocatalysis: evaluation of main intermediates and toxicity, *Environ. Sci. Technol.* 37 (2003) 2516–2524.
- [39] R.R. Solís, F.J. Rivas, A. Martínez-Piernas, A. Agüera, Ozonation, photocatalysis and photocatalytic ozonation of diuron, *Intermed. Identif. Chem. Eng. J.* 292 (2016) 72–81.
- [40] L. Zhou, W. Zheng, Y. Ji, J. Zhang, C. Zeng, Y. Zhang, Q. Wang, X. Yang, Ferrous-activated persulfate oxidation of arsenic(III) and diuron in aquatic system, *J. Hazard. Mater.* 263 (2013) 422–430.
- [41] M.V. Shankar, S. Nélieu, L. Kerhoas, J. Einhorn, Photo-induced degradation of diuron in aqueous solution by nitrites and nitrates: kinetics and pathways, *Chemosphere* 66 (2007) 767–774.
- [42] M. Carrier, C. Guillard, M. Besson, C. Bordes, H. Chermette, Photocatalytic degradation of diuron: experimental analyses and simulation of HO radical attacks by density functional theory calculations, *J. Phys. Chem. A* 113 (2009) 6365–6374.
- [43] J. Feng, Z. Zheng, Y. Sun, J. Luan, Z. Wang, L. Wang, J. Feng, Degradation of diuron in aqueous solution by dielectric barrier discharge, *J. Hazard. Mater.* 154 (2008) 1081–1089.
- [44] J. Feng, Z. Zheng, J. Luan, J. Zhang, L. Wang, Degradation of diuron in aqueous solution by ozonation, *J. Environ. Sci. Health: Part B* 43 (2008) 576–587.
- [45] H. Mestankova, B. Escher, K. Schirmer, U. von Gunten, S. Canonica, Evolution of algal toxicity during (photo)oxidative degradation of diuron, *Aquat. Toxicol.* 101 (2011) 466–473.
- [46] R.M. Ramirez Zamora, R. Seux, Oxidation du diuron et identification de quelques sous-produits de la réaction, *Revue des sciences de l'eau* 12 (1999) 545.
- [47] L.A. Tahmassebi, S. Nélieu, L. Kerhoas, J. Einhorn, Ozonation of chlorophenylurea pesticides in water: reaction monitoring and degradation pathways, *Sci. Total Environ.* 291 (2002) 33–44.
- [48] J. Jirkovský, V. Faure, P. Boule, Photolysis of diuron, *Pestic. Sci.* 50 (1997) 42–52.
- [49] K. Macounová, H. Krýsová, J. Ludvík, Jr. Jirkovský, Kinetics of photocatalytic degradation of diuron in aqueous colloidal solutions of Q-TiO₂ particles, *J. Photochem. Photobiol. A: Chem.* 156 (2003) 273–282.
- [50] P. Mazellier, J. Jirkovský, M. Bolte, Degradation of diuron photoinduced by iron (III) in aqueous solution, *Pestic. Sci.* 49 (1997) 259–267.
- [51] M.A. Oturan, N. Oturan, M.C. Edelahy, F.I. Podvorica, K.E. Kacemi, Oxidative degradation of herbicide diuron in aqueous medium by Fenton's reaction based advanced oxidation processes, *Chem. Eng. J.* 171 (2011) 127–135.
- [52] M. Carrier, M. Besson, C. Guillard, E. Gonze, Removal of herbicide diuron and thermal degradation products under catalytic wet air oxidation conditions, *Appl. Catal. B: Environ.* 91 (2009) 275–283.
- [53] F.-X. Tian, B. Xu, T.-Y. Zhang, N.-Y. Gao, Degradation of phenylurea herbicides by chlorine dioxide and formation of disinfection by-products during subsequent chl (am)ination, *Chem. Eng. J.* 258 (2014) 210–217.
- [54] J. Feng, Z. Zheng, J. Luan, K. Li, L. Wang, J. Feng, Gas-liquid hybrid discharge-induced degradation of diuron in aqueous solution, *J. Hazard. Mater.* 164 (2009) 838–846.
- [55] M.J. Farré, S. Brosillon, X. Domènech, J. Peral, Evaluation of the intermediates generated during the degradation of diuron and linuron herbicides by the photo-Fenton reaction, *J. Photochem. Photobiol. A: Chem.* 189 (2007) 364–373.
- [56] A.R.F. Pipi, I. Sirés, A.R. De Andrade, E. Brillas, Application of electrochemical advanced oxidation processes to the mineralization of the herbicide diuron, *Chemosphere* 109 (2014) 49–55.
- [57] G. Mascolo, A. Lopez, H. James, M. Fielding, By-products formation during degradation of isoproturon in aqueous solution. I: ozonation, *Water Res.* 35 (2001) 1695–1704.
- [58] G. Mascolo, A. Lopez, H. James, M. Fielding, By-products formation during degradation of isoproturon in aqueous solution. II: chlorination, *Water Res.* 35 (2001) 1705–1713.
- [59] M.V.P. Sharma, V. Durgakumari, M. Subrahmanyam, Solar photocatalytic degradation of isoproturon over TiO₂/H-MOR composite systems, *J. Hazard. Mater.* 160 (2008) 568–575.
- [60] A. Amorisco, I. Losito, F. Palmisano, P.G. Zamboni, Photocatalytic degradation of the herbicide isoproturon: characterisation of by-products by liquid chromatography with electrospray ionisation tandem mass spectrometry, *Rapid Commun. Mass Spectrom.* 19 (2005) 1507–1516.
- [61] I. Losito, A. Amorisco, F. Palmisano, Electro-Fenton and photocatalytic oxidation of phenyl-urea herbicides: an insight by liquid chromatography–electrospray ionization tandem mass spectrometry, *Appl. Catal. B: Environ.* 79 (2008) 224–236.
- [62] M.J. López-Muñoz, A. Revilla, J. Aguado, Heterogeneous photocatalytic degradation of isoproturon in aqueous solution: experimental design and intermediate products analysis, *Catal. Today* 209 (2013) 99–107.
- [63] A. Lopez, G. Mascolo, G. Tiravanti, R. Passino, Degradation of herbicides (ametryn and isoproturon) during water disinfection by means of two oxidants (hypochlorite and chlorine dioxide), *Water Sci. Technol.* 35 (1997) 129–136.
- [64] H. Allemann, M. Prados-Ramirez, J.P. Croué, B. Legube, Recherche et identification des premiers sous-produits d'oxydation de l'isoproturon par le système ozone/peroxyde d'hydrogène, *Revue des sciences de l'eau* 8 (1995) 315.